Check for updates

# Two new phases in the ternary RE–Ga–S systems with the unique interlinkage of GaS₄ building units: synthesis, structure, and properties†

Hua Lin, ‡[a] Jin-Ni Shen,‡[b] Wei-Wei Zhu, [c] Yi Liu, *[c] Xin-Tao Wu,[a] Qi-Long Zhu *[a] and Li-Ming Wu *[a,d]

Two novel ternary rare-earth chalcogenides, $Yb_6Ga_4S_{15}$ and $Lu_5GaS_9$, have been prepared by solid-state reactions of an elemental mixture at high temperatures. Their structures were determined on the basis of single-crystal X-ray diffraction. $Yb_6Ga_4S_{15}$ crystallizes in the monoclinic space group $C2/m$ (no.12) [$a$ = 23.557(2) Å, $b$ = 3.7664(4) Å, $c$ = 12.466(1) Å, $\beta$ = 90.915(9)°, $V$ = 1105.9(2) Å³ and $Z$ = 2], whereas $Lu_5GaS_9$ crystallizes in the triclinic space group $P\bar{1}$ (no.2) [$a$ = 7.735(3) Å, $b$ = 10.033(4) Å, $c$ = 10.120(4) Å, $\alpha$ = 106.296(4)°, $\beta$ = 100.178(5)°, $\gamma$ = 101.946(3)°, $V$ = 714.1(5) Å³ and $Z$ = 2]. Both the structures feature complicated three dimensional frameworks with the unique interlinkages of GaS₄ as basic building units. Significantly, photo-electrochemical measurements indicated that title compounds were photoresponsive under visible-light illumination. Furthermore, the UV–visible–near IR diffuse reflectance spectra, thermal stabilities, electronic structures, physical properties as well as a structure change trend of the ternary rare-earth/gallium/sulfur compounds have been evaluated.

## Introduction

Recently, quaternary chalcogenides that contain a rare-earth metal together with a group 13 main-group metal (*e.g.*, Ga and In) are of great interest due to their fascinating structural chemistry and interesting physical properties including magnetic, photo-response, photoelectric, and nonlinear optical (NLO) properties.[1–18] For example, 1D infinite anionic chains containing the compound $Ba_2REMQ_5$ (RE = rare-earth metal; M = Ga, In; Q = S, Se, Te) offer flexibility in band gap engineering by controlling the composition and show weak short-range antiferromagnetic interactions between the adjacent $RE^{3+}$ cations.[7,9,10] $La_3CuGaSe_7$ contains interesting isolated $[CuSe_3]^{4-}$ pyramids and

$[GaSe_4]^{5-}$ tetrahedra and exhibits interesting centrosymmetric photo-response behaviour.[15] The $CuIn_{1-x}Ce_xTe_2$ film shows excellent photoelectric properties and has potential applications as a competent absorber material in photovoltaic devices.[16] Non-centrosymmetric $Sm_4GaSbS_9$ and $La_4InSbS_9$ exhibit very strong powder second harmonic generation (SHG) responses in the IR range, indicating that they are promising candidates for laser frequency conversion applications.[5,6]

Compared with the extensive research studies on quaternary systems, the studies on ternary rare earth metal/gallium/sulfur (RE/Ga/S) compounds are relatively scarce. The existing examples are limited to only $REGa_2S_4$ (RE = Sm, Eu, Yb),[19] $LaGaS_3$,[20] $RE_6Ga_{3.33}S_{14}$ (RE = La–Nd, Sm–Tb, Y),[21] and $RE_3GaS_6$ (RE = Dy, Ho, Er, Y).[22] From the structure point of view, all of them contain GaS₄ tetrahedra as the basic building units (BBUs), which can be further interlinked by multi-connection ways with the S atoms to create a 0D cluster, infinite 1D chain, or a 2D layer. More interestingly, the Ga–S substructure in these known ternary RE/Ga/S compounds decreases as the RE/Ga atomic ratio increases. For example, as the RE/Ga atomic ratio increases from 0.5 (for the $REGa_2S_4$ type) to 1.0 (for $LaGaS_3$) and then to 3.0 (for the $RE_3GaS_6$ type), the Ga–S sub-structure decreases from the 2D layer to the 1D zigzag chain and then to the 0D monomeric GaS₄ cluster (shown below). Such results inspire us to make further efforts to synthesize new compounds in a related system by adjusting the RE/Ga atomic ratio, especially to some extreme ratios.

[a]*State Key Laboratory of Structural Chemistry, Fujian Institute of Research on the Structure of Matter, Chinese Academy of Sciences, Fuzhou, Fujian 350002, People's Republic of China. E-mail: liuyimse@zju.edu.cn, qlzhu@fjirsm.ac.cn, liming_wu@fjirsm.ac.cn*
[b]*College of Materials Science and Engineering, Fuzhou University, Fujian 350108, People's Republic of China*
[c]*State Key Laboratory of Silicon Materials, School of Materials Science and Engineering, Zhejiang University, Hangzhou 310027, People's Republic of China*
[d]*Key Laboratory of Theoretical and Computational Photochemistry, Ministry of Education, College of Chemistry, Beijing Normal University, Beijing 100875, People's Republic of China*
†CCDC 1540907 and 1540908. For crystallographic data in CIF or other electronic format see DOI: 10.1039/c7dt02545a
‡These authors contributed equally to this work.

In this study, our detailed exploratory investigation has led to the discovery of two novel sulfides $Yb_6Ga_4S_{15}$ and $Lu_5GaS_9$ representing the new structure types in the RE/Ga/S system. The RE/Ga atomic ratio of 5.0 in the latter breaks the known high limit. The discrete dimeric $(GaS_4)_2$ tetrahedra were periodically embedded within the 3D Lu–S covalent channel. Whereas in the former, the RE/Ga atomic ratio of 1.5 lies between the known 1.0 ($LaGaS_3$) and 1.8 ($RE_6Ga_{3.33}S_{14}$ type), and it contains an unprecedented 1D $GaS_4$ double-tetra-hedron-chain. In addition, the syntheses, single crystal analyses, optical band gaps, and magnetic and photo-electro-chemical properties as well as electronic structures based on VASP calculations are reported.

## Experimental section

### Materials and instrumentation

All of the reactants were from commercial sources and used without further purification. Yb (3N) and Lu (3N) were purchased from Huhhot Jinrui Rare Earth Co., Ltd. Ga (5N) and S (5N) were purchased from Alfa Aesar. Microprobe elemental analyses were performed on a field emission scanning electron microscope (FESEM, JSM6700F) equipped with an energy dispersive X-ray spectroscope (EDX, Oxford INCA). Powder X-ray diffraction (PXRD) patterns (Cu-K$_\alpha$) were collected on a Rigaku MiniFlex II powder diffractometer. The solid-state optical absorption spectra were recorded at room temperature using a PerkinElmer Lambda 950 UV–Vis spectro-photometer and $BaSO_4$ was used as a standard. The thermal stability analyses were performed on a NETZSCH STA 449C simultaneous analyser under a nitrogen atmosphere. Magnetic susceptibility measurements were carried out using a Quantum Design PPMS-9T magnetometer at a field of 1000 Oe in the temperature range of 2–300 K. The photo-electro-chemical tests were performed using an electrochemical work-station (CHI660E) with a conventional three-electrode setup under simulated solar light illumination. The as-prepared title compounds were coated on a slice of an ITO glass with an area of $1 \times 1$ cm$^2$ and employed as the working electrode. A platinum wire and saturated $Hg/HgCl_2$ were used as the counter and reference electrodes, respectively, and a 0.2 M $Na_2SO_4$ aqueous solution was used as an electrolyte. A 500 W Xe lamp was utilized as the simulated solar light source.

### Syntheses

Two title compounds were synthesized through conventional high-temperature solid-state reactions of an elemental mixture. The loaded compositions are as follows: Yb (0.5191 g, 3 mmol), Ga (0.1394 g, 2 mmol) and S (0.2405 g, 7.5 mmol) for $Yb_6Ga_4S_{15}$, and Lu (0.4374 g, 2.5 mmol), Ga (0.0349 g, 0.5 mmol) and S (0.1443 g, 4.5 mmol) for $Lu_5GaS_9$. These mixtures were loaded into silica tubes and then flame-sealed under a high vacuum of $10^{-3}$ Pa. The sealed tubes were placed in a temperature-controlled furnace, heated to 1223 K for $Yb_6Ga_4S_{15}$ (1323 K for $Lu_5GaS_9$) for 100 h, and annealed at this
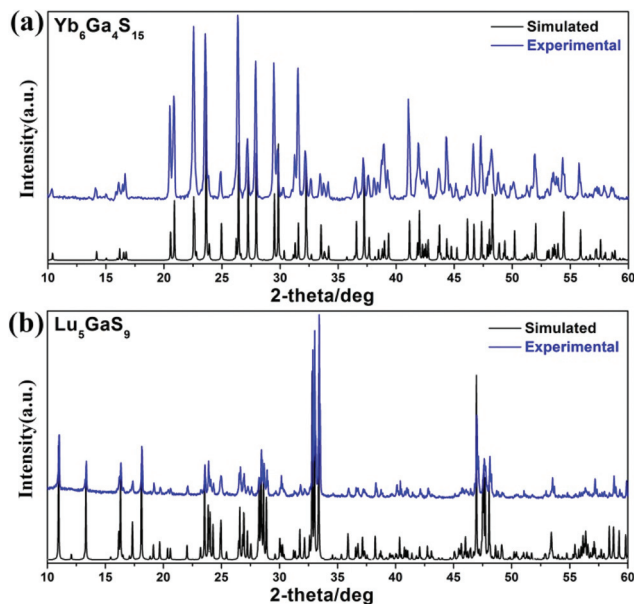


Fig. 1 Experimental (blue) and simulated (black) PXRD patterns of (a) $Yb_6Ga_4S_{15}$ and (b) $Lu_5GaS_9$.

temperature for 3 days, and then slowly cooled to 673 K at 3 K h$^{-1}$ before switching off the furnace. Their purities were confirmed by PXRD studies (see Fig. 1). The experimental PXRD patterns of the two title compounds are in agreement with the ones simulated from their single-crystal XRD data. The results of the EDX analyses of the single crystals of the title compounds gave average molar ratios of RE/Ga/S of 6/4.03(4)/15.11(2) for $Yb_6Ga_4S_{15}$ and 5/0.97(1)/9.05(4) for $Lu_5GaS_9$, respectively, which are in good agreement with those deter-mined from single-crystal XRD structural analyses. The crystals appear stable in air and moisture over the periods of time longer than three months.

### Single-crystal X-ray diffraction (XRD)

Data of the title compounds were collected on a Mercury 70 CCD diffractometer with Mo-K$_\alpha$ radiation at 293 K. The data sets were corrected for Lorentz and polarization factors as well as for absorption by the multi-scan method.[23] Two structures were solved by direct methods and refined by full-matrix least-squares fitting on $F^2$ by using the SHELX-2014 program package.[24] All of the non-hydrogen atoms were refined with anisotropic thermal parameters and the coordinates were standardized using STRUCTURE TIDY.[25] Crystallographic data and structural refinements of the title compounds are summarized in Table 1, the positional coordinates and an-isotropic parameters are shown in Table 2, and some impor-tant bond distances are listed in Table 3.

### Computational section

Utilizing density functional theory (DFT) as implemented in the Vienna *ab initio* simulation package (VASP) code,[26] we investigate the electronic structures of the title compounds.

**Table 1** Crystallographic data and refinement details of $Yb_6Ga_4S_{15}$ and $Lu_5GaS_9$

| Formula | $Yb_6Ga_4S_{15}$ | $Lu_5GaS_9$ |
|---|---|---|
| Fw | 1798.02 | 1233.11 |
| Crystal system | Monoclinic | Triclinic |
| Crystal color | Deep-red | Brown |
| Space group | $C2/m$ (no. 12) | $P\bar{1}$ (no. 2) |
| $a$ (Å) | 23.557(2) | 7.735(3) |
| $b$ (Å) | 3.7664(4) | 10.033(4) |
| $c$ (Å) | 12.466(2) | 10.120(4) |
| $\alpha$ (°) | 90 | 106.296(4) |
| $\beta$ (°) | 90.915(9) | 100.178(5) |
| $\gamma$ (°) | 90 | 101.946(3) |
| $V$ (Å³) | 1105.9(2) | 714.1(5) |
| $Z$ | 2 | 2 |
| $D_c$ (g cm⁻³) | 5.40 | 5.74 |
| $\mu$ (mm⁻¹) | 31.3 | 37.4 |
| GOOF on $F^2$ | 1.07 | 1.06 |
| $R_1$, w$R_2$ $(I > 2\sigma(I))^a$ | 0.0232, 0.0547 | 0.0241, 0.0553 |
| $R_1$, w$R_2$ (all data) | 0.0243, 0.0555 | 0.0299, 0.0582 |
| Largest diff. peak and hole (e Å⁻³) | 1.118, −1.406 | 1.830, −2.082 |

$^a R_1 = \sum ||F_o| - |F_c||/\sum|F_o|$, $wR_2 = [\sum w(F_o^2 - F_c^2)^2/\sum w(F_o^2)^2]^{1/2}$.

**Table 2** Atomic coordinates and equivalent isotropic displacement parameters of $Yb_6Ga_4S_{15}$ and $Lu_5GaS_9$

| Atom | Wyckoff | $x$ | $y$ | $z$ | $U_{(eq)}{}^a$ |
|---|---|---|---|---|---|
| **$Yb_6Ga_4S_{15}$** | | | | | |
| Yb1 | 4i | 0.51727(2) | 0 | 0.15150(4) | 0.0080(2) |
| Yb2 | 4i | 0.71101(2) | 0 | 0.23808(4) | 0.0100(2) |
| Yb3 | 4i | 0.83853(2) | 0 | 0.04540(4) | 0.0094(2) |
| Ga1 | 4i | 0.08996(5) | 0 | 0.0099(3) | 0.0099(3) |
| Ga2 | 4i | 0.36310(5) | 0 | 0.33187(9) | 0.0094(3) |
| S1 | 4i | 0.0202(2) | 0 | 0.2971(2) | 0.0107(5) |
| S2 | 4i | 0.1794(2) | 0 | 0.3676(2) | 0.0127(6) |
| S3 | 4i | 0.1905(2) | 0 | 0.6488(2) | 0.0126(6) |
| S4 | 4i | 0.2571(2) | 0 | 0.1098(2) | 0.0082(5) |
| S5 | 4i | 0.4004(2) | 0 | 0.1651(2) | 0.0095(5) |
| S6 | 4i | 0.4289(2) | 0 | 0.4716(2) | 0.0085(5) |
| S7 | 4i | 0.6272(2) | 0 | 0.0968(2) | 0.0092(5) |
| S8 | 2a | 0 | 0 | 0 | 0.0123(8) |
| **$Lu_5GaS_9$** | | | | | |
| Lu1 | 2i | 0.13901(4) | 0.34263(3) | 0.73338(3) | 0.00689(8) |
| Lu2 | 2i | 0.18990(4) | 0.67889(3) | 0.62276(3) | 0.00542(8) |
| Lu3 | 2i | 0.25093(4) | 0.00984(3) | 0.48854(3) | 0.00513(8) |
| Lu4 | 2i | 0.36329(4) | 0.64655(3) | 0.27758(3) | 0.00535(8) |
| Lu5 | 2i | 0.46198(4) | 0.30928(3) | 0.04389(3) | 0.00612(8) |
| Ga1 | 2i | 0.1238(2) | 0.90265(8) | 0.02461(8) | 0.0072(2) |
| S1 | 2i | 0.0209(2) | 0.1669(2) | 0.4603(2) | 0.0058(3) |
| S2 | 2i | 0.0821(2) | 0.5070(2) | 0.3446(2) | 0.0060(4) |
| S3 | 2i | 0.1505(2) | 0.8225(2) | 0.2193(2) | 0.0062(4) |
| S4 | 2i | 0.1728(2) | 0.1498(2) | 0.1039(2) | 0.0081(4) |
| S5 | 2i | 0.2670(2) | 0.4969(2) | 0.0053(2) | 0.0063(4) |
| S6 | 2i | 0.3587(2) | 0.1768(2) | 0.7644(2) | 0.0055(3) |
| S7 | 2i | 0.5476(2) | 0.1675(2) | 0.4557(2) | 0.0049(3) |
| S8 | 2i | 0.5869(2) | 0.4823(2) | 0.3163(2) | 0.0058(3) |
| S9 | 2i | 0.6846(2) | 0.1591(2) | 0.1089(2) | 0.0085(4) |

$^a U_{(eq)}$ is defined as one-third of the trace of the orthogonalized $U_{ij}$ tensor.

We used the projector augmented wave (PAW)[27] method for the ionic cores and the generalized gradient approximation (GGA)[28] for the exchange–correlation potential, in which the

**Table 3** Selected bond lengths (Å) of $Yb_6Ga_4S_{15}$ and $Lu_5GaS_9$

| $Yb_6Ga_4S_{15}$ | | $Lu_5GaS_9$ | | | |
|---|---|---|---|---|---|
| Yb1–S1 × 2 | 2.616(2) | Lu1–S1 | 2.699(2) | Lu4–S2 | 2.636(2) |
| Yb1–S5 | 2.761(2) | Lu1–S2 | 2.662(2) | Lu4–S3 | 2.761(2) |
| Yb1–S7 | 2.687(2) | Lu1–S3 | 2.698(2) | Lu4–S5 | 2.626(2) |
| Yb1–S8 × 2 | 2.693(4) | Lu1–S5 | 2.638(2) | Lu4–S6 | 2.667(2) |
| Yb2–S2 × 2 | 2.597(2) | Lu1–S6 | 2.652(2) | Lu4–S7 | 2.689(2) |
| Yb2–S3 | 2.697(3) | Lu1–S8 | 2.677(2) | Lu4–S8 | 2.677(2) |
| Yb2–S4 × 2 | 2.709(2) | Lu2–S1 | 2.656(2) | Lu5–S4 | 2.734(2) |
| Yb2–S7 | 2.625(3) | Lu2–S2 | 2.642(2) | Lu5–S5 | 2.766(2) |
| Yb3–S4 × 2 | 2.815(2) | Lu2–S2 | 2.728(2) | Lu5–S5 | 2.711(2) |
| Yb3–S7 × 2 | 2.718(2) | Lu2–S7 | 2.663(2) | Lu5–S6 | 2.657(2) |
| Yb3–S5 × 2 | 2.798(2) | Lu2–S8 | 2.704(2) | Lu5–S8 | 2.688(2) |
| Yb3–S4 | 2.945(2) | Lu2–S9 | 2.626(2) | Lu5–S9 | 2.626(2) |
| Ga1–S1 | 2.255(3) | Lu3–S1 | 2.655(3) | Ga1–S3 | 2.321(2) |
| Ga1–S2 | 2.227(3) | Lu3–S1 | 2.639(2) | Ga1–S4 | 2.300(2) |
| Ga1–S6 × 2 | 2.343(2) | Lu3–S1 | 2.681(2) | Ga1–S4 | 2.308(2) |
| Ga2–S3 × 2 | 2.282(2) | Lu3–S3 | 2.708(2) | Ga1–S9 | 2.242(2) |
| Ga2–S5 | 2.270(3) | Lu3–S7 | 2.634(2) | | |
| Ga2–S6 | 2.313(3) | Lu3–S7 | 2.704(2) | | |

Perdew–Burke–Ernzerhof (PBE)[29] type exchange–correlation was adopted. The reciprocal space was sampled with a 0.03 Å⁻¹ spacing in the Monkhorst–Pack scheme for structure optimization, while denser $k$-point grids with a 0.01 Å⁻¹ spacing were adopted for property calculation. We used a mesh cut-off energy of 500 eV to determine the self-consistent charge density. All geometries are fully relaxed until the Hellmann–Feynman force on atoms is less than 0.01 eV Å⁻¹ and the total energy change is less than $1.0 \times 10^{-5}$ eV.

## Results and discussion

The novel ternary $Yb_6Ga_4S_{15}$ phase crystallizes in the centrosymmetric space group $C2/m$ (Pearson symbol $mC50$, no.12) [$a = 23.557(2)$ Å, $b = 3.7664(4)$ Å, $c = 12.466(1)$ Å, $\beta = 90.915(9)°$, $V = 1105.9(2)$ Å³ and $Z = 2$]. There are 13 unique crystallographic positions in the asymmetric unit of the structure, including three Yb sites, two Ga sites and eight S sites (Table 2). As shown in Fig. 2, the remarkable structural feature is the novel 3D framework based on the 2D Yb–S layers of the two different corner-sharing substructures (chain A and chain B), which are further bridged by 1D $GaS_4$ double-tetrahedron-chains extending along the $c$ direction. Each chain A is composed of condensed $Yb1S_6$ octahedra via sharing of 4-fold $\mu_4$-S8 bridging atoms (shared by four coplanar octahedra) and 2-fold $\mu_2$-S2 bridging atoms (shared by two coplanar octahedra), as shown in Fig. 3a. $Yb2S_6$ octahedra and $Yb3S_7$ mono-capped trigonal prisms are interconnected via corner-sharing (S2, S4, S5 and S7) into a double chain along the $b$-axis. Then, such two 1D chains are alternately interconnected via corner-sharing (S4), resulting in the formation of chain B (Fig. 3a). All Yb–S bonds range from 2.597(2) to 2.945(2) Å (Table 3), which are close to the Yb–S bonds in $Yb_2S_3$ (2.672–2.733 Å),[30] $YbPS_4$ (2.816–2.964 Å)[31] and $Yb_2BiS_4$ (2.858–2.985 Å).[32] Each infinite 1D $GaS_4$ double-tetrahedron-chain is formed by corner-sharing $Ga1S_4$ tetrahedra and $Ga2S_4$ tetrahedra, as shown in Fig. 3b.

**Paper**
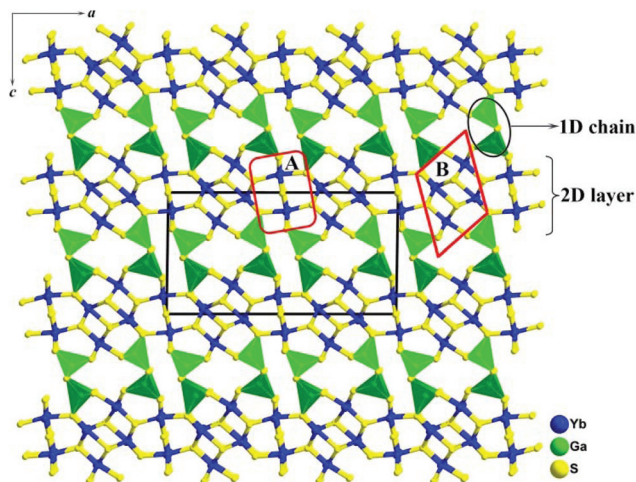
**Fig. 2** Crystal structure of $Yb_6Ga_4S_{15}$ with the unit cell marked viewed parallel to [010]. The structure is formed by 1D Ga−S chains and 2D Yb−S layers. The 2D layer consists of two different substructures (chain A and chain B) which are alternately connected along the $a$ axis (the details are shown in Fig. 3).
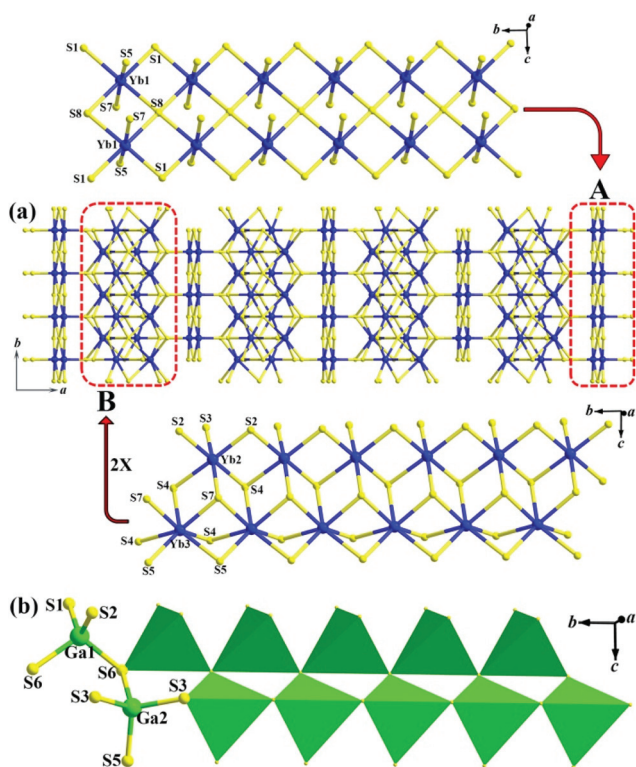


**Fig. 3** (a) Approximate [001] structure view of the 2D Yb−S layer in $Yb_6Ga_4S_{15}$. Chain A is composed of condensed $Yb1S_6$ octahedra, whereas the single-chain in chain B consists of $Yb2S_6$ octahedra and $Yb3S_7$ mono-capped trigonal prisms. (b) $GaS_4$ double-tetrahedron-chain extending along the $c$ direction in $Yb_6Ga_4S_{15}$.

Remarkably, such a double $GaS_4$ tetrahedron 1D chain is observed for the first time in the ternary RE/Ga/S system. The Ga−S distances vary from 2.227(3) to 2.343(2) Å (Table 3),
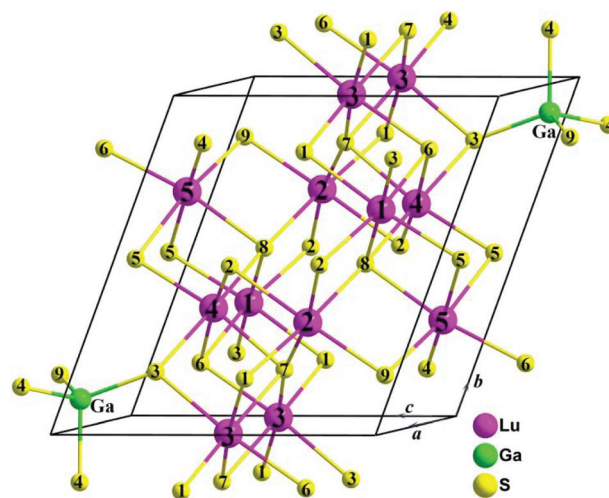


**Fig. 4** Structure of $Lu_5GaS_9$ with the atom number and unit cell marked.

which are close to those in $YbGa_2S_4$ (2.269–2.281 Å)[19c] and β-$LaGaS_3$ (2.194–2.325 Å).[20a]

The unit cell of $Lu_5GaS_9$ is shown in Fig. 4. It has the largest RE/Ga molar ratio in the RE/Ga/S system reported so far and crystallizes in the triclinic space group $P\bar{1}$ (Pearson symbol $aP30$, no.2) [$a$ = 7.735(3) Å, $b$ = 10.033(4) Å, $c$ = 10.120(4) Å, $\alpha$ = 106.296(4)°, $\beta$ = 100.178(5)°, $\gamma$ = 101.946(3)°, $V$ = 714.1(5) Å³ and $Z$ = 2]. In the structure, there are 15 crystallographically unique atoms (including 5 Lu atoms, 1 Ga atom and 9 S atoms) in the asymmetric unit and all are in special positions (Table 2). All Lu atoms are 6-fold coordinated in distorted $LuS_6$ octahedra with Lu−S bonds ranging from 2.626(2) to 2.766(2) Å, which are also comparable to those in $CsLu_7S_{11}$ (2.579–2.816 Å),[33] $LuCuS_2$ (2.630–2.741 Å)[34] and $Lu_2CrS_4$ (2.602–2.695 Å),[35] as well as the sum of the ionic radii of $Lu^{3+}$ and $S^{2-}$ (2.701 Å).[36] The S−Lu−S angular deviations are ranging from 84.8 to 99.4° and 169.8 to 177.5°, respectively. Different from the discussion above, it is amazing that discrete dimeric $(GaS_4)_2$ tetrahedra can serve as the centred species in the 3D anionic Lu−S channel in the $Lu_5GaS_9$ compound. Moreover, red atoms in Fig. 5 indicate the distribution of such centred species in the unit cell, which is distributed with a large interval, at least 7.4 Å apart. In more detail, as shown in Fig. 6, dimeric $(GaS_4)_2$ tetrahedra are interconnected via corner-sharing (S3, S4 and S9) into a complete 3D Lu−Ga−S framework. Such discrete dimeric $(GaS_4)_2$ tetrahedra are observed for the first time in the ternary RE/Ga/S systems.

## Comparison with other sulfides in the RE/Ga/S system

The six RE/Ga/S structure types are shown in Fig. 7, which clearly displays a relationship between the crystal structure and the RE/Ga atomic ratio. All of the compounds contain $GaS_4$ tetrahedra as the smallest BBU. It is easily understood from this illustration that as the system contains more RE atoms, the Ga−S sub-structure is reduced. For example, the RE/
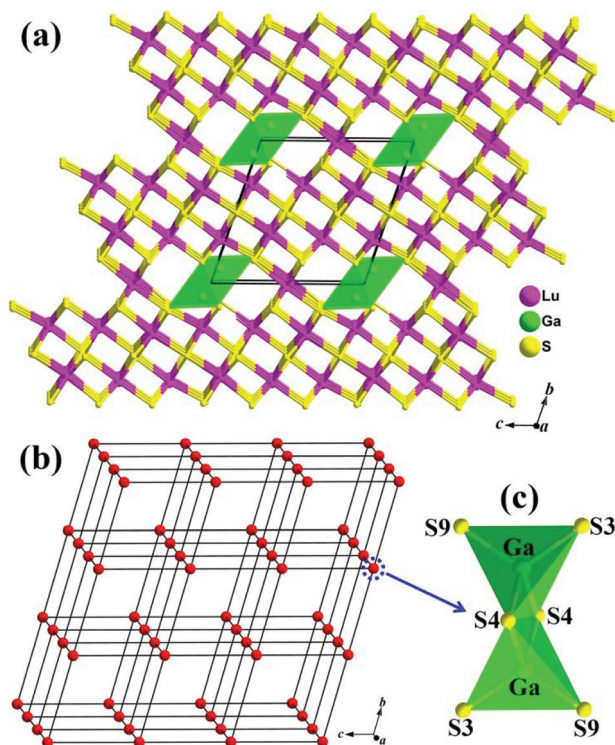
**Fig. 5** (a) Structure of $Lu_5GaS_9$ viewed along the $a$-direction showing a 3D Lu–S channel formed by 6-folded coordinated Lu metals. The discrete dimeric $(GaS_4)_2$ tetrahedra (green polyhedron) are embedded in such a channel. (b) Topological representation of dimeric $(GaS_4)_2$ tetrahedra (red atoms) in the structure with the unit cell outlined. (c) The dimeric $(GaS_4)_2$ tetrahedra with the atom number marked.
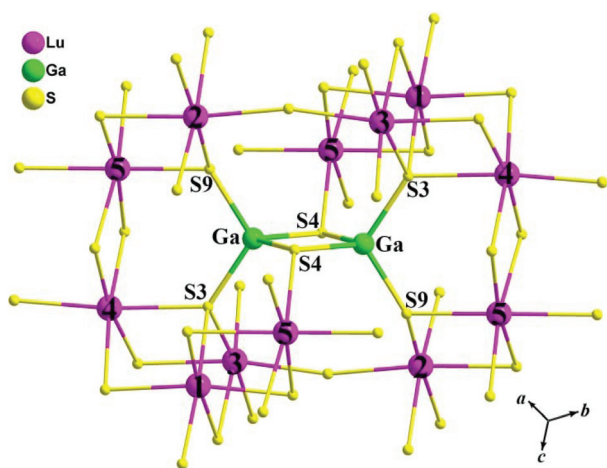


**Fig. 6** The coordination environment of dimeric $(GaS_4)_2$ tetrahedra with the surrounding Lu number outlined.

Ga ratios in $REGa_2S_4$ and $REGaS_3$ are 0.5 and 1.0, respectively, and they have 2D and 1D structures, respectively. 2D type structures are formed at the top of the figure, whereas 0D structures appear at the bottom. This can be geometrically explained. Sulfur atoms in the 2D Ga–S structures can coordi-
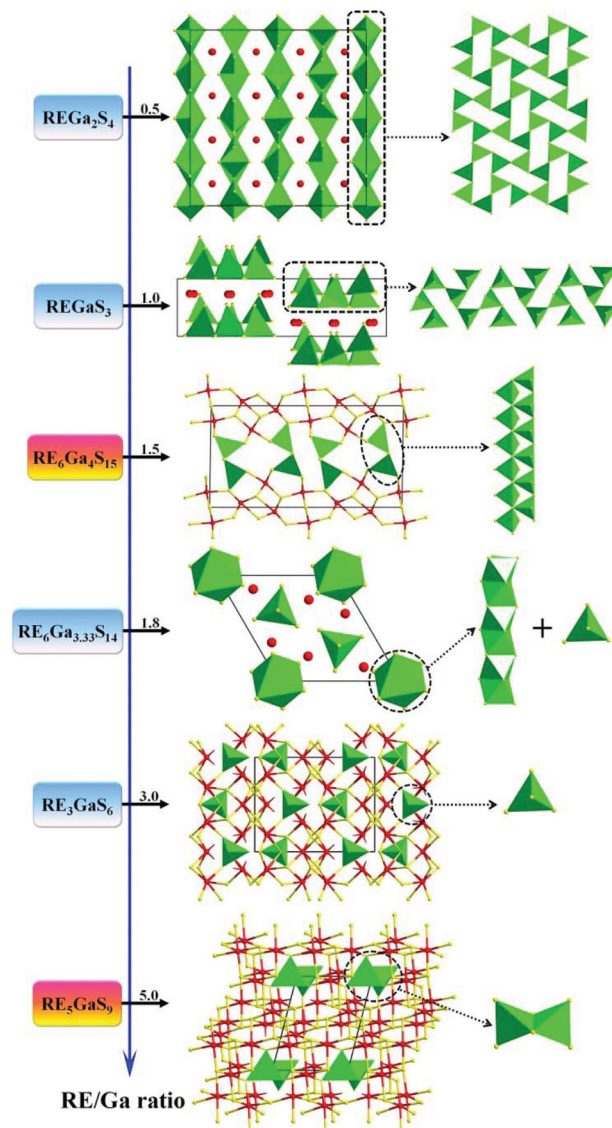


**Fig. 7** Relationship between the structure and the RE/Ga atomic ratio in the ternary RE/Ga/S system. As the RE/Ga ratio increases (bottom), the Ga–S sub-structure changes from a 2D layered structure to a 1D chain structure and then to a 0D isolated unit. Red: RE; yellow: S; green polyhedron: $GaS_4$ tetrahedra.

nate to two Ga atoms, like as in $REGa_2S_4$. In the 0D Ga–S structures, however, all of the sulfur atoms should coordinate to only one Ga atom. Therefore, as the RE/Ga atomic ratio increases, the Ga–S sub-structure generally changes from a 2D layered structure to a 1D chain structure, and then to discrete clusters.

## Thermal, magnetic and optical properties

In order to investigate the structural stability, the thermogravimetric (TG) and differential thermal analysis (DTA) experiments were performed on the title compounds. As shown in Fig. 8a and b, both compounds have excellent thermal stabilities. The TG data indicate negligible weight loss in the whole
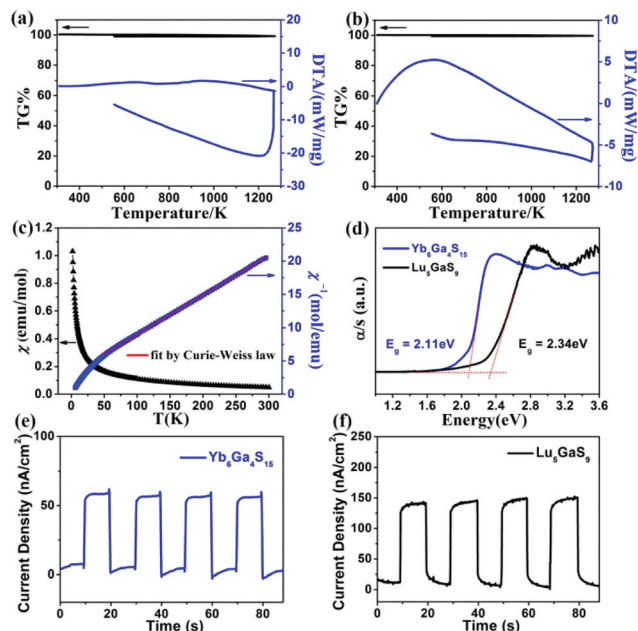
**Fig. 8** TG (black) and DTA (blue) diagrams of (a) $Yb_6Ga_4S_{15}$ and (b) $Lu_5GaS_9$. (c) Temperature ($T$) dependence of the molar magnetic susceptibility ($\chi$) and the inverse molar magnetic susceptibility ($\chi^{-1}$) for $Yb_6Ga_4S_{15}$. (d) Solid-state UV-vis optical absorption spectra of $Yb_6Ga_4S_{15}$ (blue line) and $Lu_5GaS_9$ (black line). Photocurrent responses of (e) $Yb_6Ga_4S_{15}$ and (f) $Lu_5GaS_9$ under simulated solar light illumination.

measured temperature range (300–1273 K) and no melting or phase transition processes can be identified from the corresponding DTA cycling curves.

The magnetic susceptibility of the compound $Yb_6Ga_4S_{15}$ is shown in Fig. 8c, which is collected at an applied field of 1000 Oe. Since $Ga^{3+}$ and $S^{2-}$ are diamagnetic species, the magnetic (paramagnetism) contribution is expected to originate from the $Yb^{3+}$ ions. Linear fitting of the molar susceptibility ($1/\chi$) with $T$ in the temperature range of 50–300 K indicates a Curie constant ($C$) of 15.23 emu K mol$^{-1}$ and a Weiss constant ($\theta$) of −47.96 K. The theoretical total effective magnetic moment in the temperature region can be calculated by using the equation $\mu_{eff}$ (total) $= [6\mu_{eff} (Yb)^2]^{1/2}$ and is found to be 11.61$\mu_B$, which is comparable to the experimental effective magnetic moment 11.04$\mu_B$. The large negative $\theta$ value suggests strong antiferromagnetic interactions existing between the $Yb^{3+}$ ions.

Fig. 8d shows the UV–vis–NIR diffuse reflectance spectra of the title compounds. The results show that the polycrystalline title compounds possess semiconducting band gaps of 2.11 eV (for $Yb_6Ga_4S_{15}$) and 2.34 eV (for $Lu_5GaS_9$), which are confirmed by the colour of the obtained crystal.

The photo-electrochemical properties of the title compounds were also studied in a three-electrode set-up, including a working electrode ($Yb_6Ga_4S_{15}$ or $Lu_5GaS_9$), a saturated $Hg/HgCl_2$ reference electrode and a Pt-wire counter electrode. Fig. 8e and f show the rapid and consistent photocurrent responses of $Yb_6Ga_4S_{15}$ and $Lu_5GaS_9$ for each switch-on and -off event in multiple 10 s on–off cycles under simulated solar

light illumination. The steady state of both compounds reached less than 1 s when the light was switched on, indicating that these two compounds possess a high transfer efficiency of photo-generated electrons and a separation efficiency of photo-generated electron–hole pairs.[37–44] Moreover, $Lu_5GaS_9$ exhibits a stronger transient photocurrent response which is about 3 times larger than that of $Yb_6Ga_4S_{15}$. These data are smaller than those of $ReSe_8Br_2$ (9 µA cm$^{-2}$),[45] CuSnSe-1 (3 µA cm$^{-2}$),[46] $[Ru(bpy)_3][Cd_{17}S_4(SPh)_{28}]$ (0.6 µA cm$^{-2}$),[40] and $ReS_8Br_2$ (0.3 mA cm$^{-2}$),[45] but wider than those of $BaCuSbS_3$ (55 nA cm$^{-2}$)[44] and $BaCuSbSe_3$ (30 nA cm$^{-2}$).[44]

### Theoretical studies

The first-principles electronic band structures of the title compounds are studied (Fig. 9a and b). The calculations indicate the semiconductor characteristics, and the calculated energy gaps ($E_g$) are 1.45 and 1.89 eV for $Yb_6Ga_4S_{15}$ (direct band-gap) and $Lu_5GaS_9$ (indirect band-gap), respectively, which are smaller than the experimental results (2.11 eV for $Yb_6Ga_4S_{15}$ and 2.34 eV for $Lu_5GaS_9$). Such a discrepancy is due to the discontinuity of the exchange–correlation energy implemented in the GGA calculation.[28] The partial density of states (PDOSs) projected on the constituent elements of the title compounds are shown in Fig. 9c and d. It is clear that the distributions of states near $E_F$ are similar for both compounds. The top of the valence bands (VBs) is mostly made up of S 3p states mixed with a small amount of the Yb or Lu 5d states and Ga 4s/4p states, whereas the bottom of the conduction bands (CBs) consists mostly of Yb or Lu 5d states and S 3p states. Since the optical response of a crystal mainly originates from the electronic transitions between the VB top and CB bottom states, thus, both compounds have similar band gaps, and the difference comes from the different energy level of Ga 4s and 4p states. The covalent bonding interactions between RE and S atoms are pretty strong according to PDOSs.
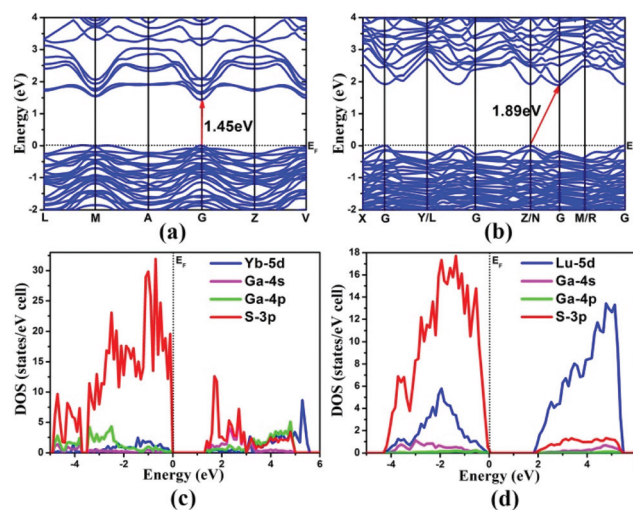


**Fig. 9** Calculated band structures of (a) $Yb_6Ga_4S_{15}$ and (b) $Lu_5GaS_9$. PDOSs of (c) $Yb_6Ga_4S_{15}$ and (d) $Lu_5GaS_9$ (the orbitals with minor contributions are omitted for clarity). The Fermi level $E_F$ is set at 0.0 eV.

## Conclusions

In summary, $Yb_6Ga_4S_{15}$ and $Lu_5GaS_9$ representing two unprecedented phases in the RE–Ga–S system have been successfully prepared by solid-state reactions at high temperatures and structurally characterized for the first time. Both of them feature complicated 3D frameworks with different connections of $GaS_4$ basic building units. Interestingly, the photo-electrochemical studies indicate that the title compounds are photoresponsive under simulated solar light illumination. In addition, the electronic structure studies reveal that the transitions from S 3p states to RE-5d and Ga 4s/4p states determine the energy gaps. Therefore, the title compounds have similar $E_g$, and the small difference comes from the different contribution of Ga 4s and Ga 4p. More interestingly, these two types together with the previously reported RE/Ga/S compounds demonstrate a nice structure change trend: as the RE/Ga atomic ratio increases, the Ga–S sub-structure generally changes from a 2D layered structure to a 1D chain structure and then to discrete $GaS_4$ tetrahedra or dimeric $(GaS_4)_2$ tetrahedra. Further studies on the understanding of the structure–property relationship and the design or prediction of new compounds in a related system are in progress.

## Conflicts of interest

There are no conflicts to declare.

## Acknowledgements

## Notes and references

1 J. D. Carpenter and S. J. Hwu, *Chem. Mater.*, 1992, **4**, 1368–1372.

2 M. R. Huch, L. D. Gulay and I. D. Olekseyuk, *J. Alloys Compd.*, 2007, **439**, 156–161.

3 A. Choudhury and P. K. Dorhout, *Inorg. Chem.*, 2008, **47**, 3603–3609.

4 S. P. Guo, G. C. Guo and J. S. Huang, *Sci. China, Ser. B*, 2009, **52**, 1609–1615.

5 M. C. Chen, P. Li, L. J. Zhou, L. H. Li and L. Chen, *Inorg. Chem.*, 2011, **50**, 12402–12404.

6 M. C. Chen, L. H. Li, Y. B. Chen and L. Chen, *J. Am. Chem. Soc.*, 2011, **133**, 4617–4624.

7 K. Feng, Y. G. Shi, W. L. Yin, W. D. Wang, J. Y. Yao and Y. C. Wu, *Inorg. Chem.*, 2012, **51**, 11144–11149.

8 H. J. Zhao, Y. F. Zhang and L. Chen, *J. Am. Chem. Soc.*, 2012, **134**, 1993–1995.

9 W. L. Yin, K. Feng, W. D. Wang, Y. G. Shi, W. Y. Hao, J. Y. Yao and Y. C. Wu, *Inorg. Chem.*, 2012, **51**, 6860–6867.

10 W. L. Yin, W. D. Wang, L. Bai, K. Feng, Y. G. Shi, W. Y. Hao, J. Y. Yao and Y. C. Wu, *Inorg. Chem.*, 2012, **51**, 11736–11744.

11 P. Wang and H. Lin, *Chinese J. Struct. Chem.*, 2013, **32**, 1873–1879.

12 W. L. Yin, W. D. Wang, L. Kang, Z. S. Lin, Y. G. Shi, W. Y. Hao, J. Y. Yao and Y. C. Wu, *J. Solid State Chem.*, 2013, **202**, 269–275.

13 W. L. Yin, Y. G. Shi, B. Kang, J. G. Deng, J. Y. Yao and Y. C. Wu, *J. Solid State Chem.*, 2014, **203**, 87–92.

14 B. W. Rudyk, S. S. Stoyko, A. O. Oliynyk and A. Mar, *J. Solid State Chem.*, 2014, **210**, 79–88.

15 X. Zhang, W. Chen, D. J. Mei, C. Zheng, F. H. Liao, Y. T. Li, J. H. Lin and F. Q. Huang, *J. Alloys Compd.*, 2014, **610**, 671–675.

16 L. Hu and Y. Q. Guo, *Chin. Phys. B.*, 2014, **23**, 127801.

17 A. K. Iyer, B. W. Rudyk, X. S. Lin, H. Singh, A. Z. Sharma, C. R. Wiebe and A. Mar, *J. Solid State Chem.*, 2015, **229**, 150–159.

18 Y. F. Shi, Y. K. Chen, M. C. Chen, L. M. Wu, H. Lin, L. J. Zhou and L. Chen, *Chem. Mater.*, 2015, **27**, 1876–1884.

19 (*a*) T. E. Peters and J. A. Baglio, *J. Electrochem. Soc.*, 1972, **119**, 230–236; (*b*) R. Roques, R. Rimet, J. P. Declercq and G. Germain, *Acta Crystallogr., Sect. B: Struct. Crystallogr. Cryst. Chem.*, 1979, **35**, 555–557; (*c*) G. G. Guseinov, F. K. Mamedov, I. R. Amiraslanov and K. S. Mamedov, *Z. Kristallogr.*, 1983, **28**, 513–515; (*d*) O. A. Aliyeva and O. M. Aliev, *Bull. Soc. Chim. Fr.*, 1986, **1**, 29–31.

20 (*a*) M. Julien-Pouzol, S. Jaulmes and C. Dagron, *Acta Crystallogr., Sect. B: Struct. Crystallogr. Cryst. Chem.*, 1982, **38**, 1566–1568; (*b*) P. Li, L. H. Li, L. Chen and L. M. Wu, *J. Solid State Chem.*, 2010, **183**, 444–450.

21 (*a*) D. De Saint-Giniez, P. Laruelle and J. Flahaut, *C. R. Acad. Sci., Ser. C*, 1968, **267**, 1029–1032; (*b*) L. G. Keiserukhskaya, N. P. Luzhnaya and Z. S. Karaev, *Inorg. Mater.*, 1970, **6**, 1869–1871; (*c*) A. M. Loireau-Lozach, M. Guittard and J. Flahaut, *Mater. Res. Bull.*, 1977, **12**, 881–886; (*d*) I. B. Bakhtiyarov and Z. D. Melikova, *Russ. J. Inorg. Chem.*, 1988, **33**, 307–309.

22 S. Jaulmes and P. Laruelle, *Acta Crystallogr., Sect. B: Struct. Crystallogr. Cryst. Chem.*, 1973, **29**, 352–354.

23 *Crystal Clear, version 1.3.5*, Rigaku Corp., The Woodlands, TX, 1999.

24 G. M. Sheldrick, *Acta Crystallogr., Sect. A: Found. Crystallogr.*, 2008, 112–122.

25 L. M. Gelato and E. Parthe, *J. Appl. Crystallogr.*, 1987, **20**, 139–143.

26 G. Kresse and J. Furthmüller, *Phys. Rev. B: Condens. Matter*, 1996, **54**, 11169–11186.

27 G. Kresse and D. Joubert, *Phys. Rev. B: Condens. Matter*, 1999, **59**, 1758–1775.

28 P. E. Blöchl, *Phys. Rev. B: Condens. Matter*, 1994, **50**, 17953–17979.

29 J. P. Perdew, K. Burke and M. Ernzerhof, *Phys. Rev. Lett.*, 1996, **77**, 3865–3868.

30 T. Schleid and F. Lissner, *J. Alloys Compd.*, 1992, **189**, 69–74.

31 K. K. Palkina, T. B. Kuvshinova, S. I. Maksimova, N. T. Chibiskova and T. A. Tripol'skaya, *Inorg. Mater.*, 1989, **25**, 1315–1316.

32 O. M. Aliev, T. F. Maksudova, N. D. Samsonova, L. D. Finkelstein and P. G. Rustamov, *Inorg. Mater.*, 1986, **22**, 23–27.

33 H. Lin, L. H. Li and L. Chen, *Inorg. Chem.*, 2012, **51**, 4588–4596.

34 S. Strobel and T. Schleid, *Z. Naturforsch., B: Chem. Sci.*, 2007, **62**, 15–22.

35 K. Tezuka, M. Wakeshima, M. Nozawa, K. Oshikane, K. Ohoyama, Y. J. Shan, H. Imoto and Y. Hinatsu, *Inorg. Chem.*, 2015, **54**, 9802–9809.

36 R. D. Shannon, *Acta Crystallogr., Sect. A: Cryst. Phys., Diffr., Theor. Gen. Cryst.*, 1976, **32**, 751–767.

37 Q. C. Zhang, Y. Liu, X. H. Bu, T. Wu and P. Y. Feng, *Angew. Chem., Int. Ed.*, 2008, **47**, 113–116.

38 Q. C. Zhang, C. D. Malliakas and M. G. Kanatzidis, *Inorg. Chem.*, 2009, **48**, 10910–10912.

39 Q. P. Luo, X. Y. Yu, B. X. Lei, H. Y. Chen, D. B. Kuang and C. Y. Su, *J. Phys. Chem. C*, 2012, **116**, 8111–8117.

40 Y. Liu, Q. P. Lin, Q. C. Zhang, X. H. Bu and P. Y. Feng, *Chem. – Eur. J.*, 2014, **20**, 8297–8301.

41 G. Li, J. W. Miao, J. Cao, J. Zhu, B. Liu and Q. C. Zhang, *Chem. Commun.*, 2014, **50**, 7656–7658.

42 W. W. Xiong, J. W. Miao, K. Q. Ye, Y. Wang, B. Liu and Q. C. Zhang, *Angew. Chem., Int. Ed.*, 2015, **54**, 546–550.

43 J. K. Gao, J. W. Miao, Y. X. Li, R. Ganguly, Y. Zhao, O. Lev, B. Liu and Q. C. Zhang, *Dalton Trans.*, 2015, **44**, 14354–14358.

44 C. Liu, P. P. Hou, W. X. Chai, J. W. Tian, X. R. Zheng, Y. Y. Shen, M. J. Zhi, C. M. Zhou and Y. Liu, *J. Alloys Compd.*, 2016, **679**, 420–425.

45 C. Fischer, N. Alonso-Vante, S. Fiechter, H. Tributsch, G. Reck and W. Schulz, *J. Alloys Compd.*, 1992, **178**, 305–314.

46 H. J. Yang, L. Wang, D. D. Hu, J. Lin, L. Luo, H. X. Wang and T. Wu, *Chem. Commun.*, 2016, **52**, 4140–4143.